UvA-DARE (Digital Academic Repository)

The fading optical counterpart of GRB 970228, 6 months and 1 year later

Fruchter, A.S.; Pian, E.; Thorsett, S.E.; Bergeron, L.E.; Gonzalez, R.A.; Metzger, M.R.; Goudfrooij, P.; Sahu, K.C.; Ferguson, H.; Livio, M.; Mutchler, M.; Petro, L.; Frontera, F.; Galama, T.J.; Groot, P.J.; Hook, R.; Kouveliotou, C.; Macchetto, D.; van Paradijs, J.A.; Palazzi, E.; Pederson, H.; Sparks, W.; Tavani, M.

THE FADING OPTICAL COUNTERPART OF GRB 970228, 6 MONTHS AND 1 YEAR LATER

Andrew S. Fruchter,[1] Elena Pian,[2] Stephen E. Thorsett,[3] Louis E. Bergeron,[1] Rosa A. González,[1] Mark Metzger,[4] Paul Goudfrooij,[1,5] Kailash C. Sahu,[1] Henry Ferguson,[1] Mario Livio,[1] Max Mutchler,[1] Larry Petro,[1] Filippo Frontera,[2,6] Titus Galama,[7] Paul Groot,[7] Richard Hook,[8] Chryssa Kouveliotou,[9] Duccio Macchetto,[1,5] Jan van Paradijs,[7] Eliana Palazzi,[2] Holger Pedersen,[10] William Sparks,[1] and Marco Tavani[11,12]

ABSTRACT

We report on observations of the fading optical counterpart of the gamma-ray burst GRB 970228, made with the *Hubble Space Telescope* (*HST*) and the Keck I telescope. The gamma-ray burst (GRB) was observed approximately 6 months after outburst, on 1997 September 4, using the *HST*/STIS CCD, and approximately 1 year after outburst, on 1998 February 24, using *HST*/NICMOS, and on 1998 April 4 using the NIRC on Keck. The unresolved counterpart is detected by STIS at $V = 28.0 \pm 0.25$, consistent with a continued power-law decline with exponent -1.10 ± 0.05. The counterpart is located within, but near the edge of, a faint extended source with diameter $\sim 0\overset{''}{.}8$ and integrated magnitude $V = 25.8 \pm 0.25$. A reanalysis of *HST* and New Technology Telescope observations performed shortly after the burst shows no evidence of proper motion of the point source or fading of the extended emission. Although the optical transient is not detected in the NICMOS images ($H \geq 25.3$), the extended source is visible and has a total magnitude $H = 23.3 \pm 0.1$. The Keck observations find $K = 22.8 \pm 0.3$. Comparison with observations obtained shortly after outburst suggests that the nebular luminosity has also been stable in the infrared. We find that several distinct and independent means of deriving the foreground extinction in the direction of GRB 970228 all agree with $A_V = 0.75 \pm 0.2$. After adjusting for this Galactic extinction, we find that the size of the observed extended emission is consistent with that of galaxies of comparable magnitude found in the Hubble Deep Field (HDF) and other deep *HST* images. Only 2% of the sky is covered by galaxies of similar or greater surface brightness. We therefore conclude that the extended source observed about GRB 970228 is almost certainly its host galaxy. Additionally, we find that independent of assumed redshift, the host is significantly bluer than typical nearby blue dwarf irregulars. With the caveat that the presently available infrared observations of the HDF are only fully complete to a limit about one-half magnitude brighter than the host, we find that the extinction-corrected $V-H$ and $V-K$ colors of the host are as blue as any galaxy of comparable or brighter magnitude in the HDF. Taken in concert with recent observations of GRB 970508, GRB 971214, and GRB 980703 our work suggests that all four GRBs with spectroscopic identification or deep multicolor broadband imaging of the host lie in rapidly star-forming galaxies.

Subject headings: gamma rays: bursts — infrared: galaxies

1. INTRODUCTION

The field of gamma-ray burst (GRB) astronomy was transformed in early 1997, when subarcminute localization of the burst GRB 970228 by the gamma- and X-ray instru-

ments on the *Beppo-SAX* satellite allowed the first firm optical identification of a fading GRB counterpart (van Paradijs et al. 1997). Within months, a second optical counterpart was found (Bond 1997; Djorgovski et al. 1997) for GRB 970508, allowing the first spectroscopic limit on the distance to a GRB, $z \geq 0.835$ (Metzger et al. 1997b). There are now nearly 10 bursts with identified optical counterparts, including three with measured redshifts.[13]

The fading counterpart of GRB 970228 remains one of the best studied of this new class of astronomical objects, but the observations have been confusing. Early *Hubble Space Telescope* (*HST*) imagery suggested the presence of a nebulosity centered $\sim 0\overset{''}{.}3$ from the pointlike fading transient source (Sahu et al. 1997b). Tentative evidence was presented that the nebular emission was fading (Metzger et al. 1997a), and a proper motion of 550 mas yr^{-1} was reported for the fading point source (Caraveo et al. 1997),

[1] Space Telescope Science Institute, 3700 San Martin Drive, Baltimore, MD 21218.

[2] Istituto di Tecnologie e Studio delle Radiazioni Extraterrestri, CNR, Via Gobetti 101, I-40129 Bologna, Italy.

[3] Joseph Henry Laboratories and Department of Physics, Princeton University, Princeton, NJ 08544.

[4] Department of Astronomy, Caltech, MS 105-24, Pasadena, CA 91125.

[5] Affiliated with the Astrophysics Division, Space Science Department, European Space Agency.

[6] Dipartimento Fisica, Università di Ferrara, Via Paradiso 12, I-44100 Ferrara, Italy.

[7] Astronomical Institute "Anton Pannekoek," University of Amsterdam, Kruislaan 403, 1098 SJ Amsterdam, Netherlands.

[8] Space Telescope European Coordinating Facility, Karl-Schwarzschild-Strasse 2, D-85748 Garching, Germany.

[9] NASA Marshall Space Flight Center, ES-84, Huntsville, AL 35812.

[10] Copenhagen University Observatory, Juliane Maries Vej 30, D-2100, Copenhagen Ä, Denmark.

[11] Columbia Astrophysics Laboratory, Columbia University, New York, NY 10027.

[12] Istituto di Fisica Cosmica e Tecnologie Relative, CNR, Via Bassini 15, I-20133 Milano, Italy.

[13] The GRB 980425 has been associated with SN1998bw. If this association is correct, then this source lies in a nearby spiral galaxy with redshift of $z = 0.008$ (Galama et al. 1998a). Its X-ray and optical luminosity would be far below that of the other GRBs with spectroscopic identification, and it most likely represents a different class of objects (Kulkarni et al. 1998b; Hogg & Fruchter 1998) from the other GRBs discussed in this work.

although the measurement was disputed (Sahu et al. 1997a). Either a fading nebula or a measurable proper motion would ineluctably lead to the conclusion that GRB 970228 was a Galactic event, unlike GRB 970508 and the other bursts with measured redshifts.

To help resolve the situation, and to further characterize the broadband spectral properties of the GRB counterpart, we have reobserved GRB 970228 with Keck and *HST*. Although the earlier *HST* observations of GRB 970228 employed WFPC2, we have availed ourselves of the newly installed STIS CCD and NICMOS camera 2. The excellent throughputs, broad bandpasses and wide spectral coverage of these instruments, combined with the long-time baseline since the gamma-ray burst, provide us with a superb opportunity to study the nature of the source and its environment.

2. OBSERVATIONS AND IMAGE ANALYSIS

2.1. *The STIS Images*

The field of GRB 970228 was imaged during two *HST* orbits on 1997 September 4 from 15:50:33 to 18:22:41 UT, using the STIS CCD in clear aperture (50CCD) mode. Two exposures of 575 s each were taken at each of four dither positions for a total exposure time of 4600 s. The exposures were dithered to allow removal of hot pixels and to obtain the highest possible resolution. The images were bias and dark subtracted and flat-fielded using the STIS pipeline. The final image was created and cleaned of cosmic rays and hot pixels using the variable pixel linear reconstruction algorithm (aka Drizzle) developed for the Hubble Deep Field (HDF) (Williams et al. 1996; Fruchter & Hook 1997).

The photometric calibration of the images was performed using the synthetic photometry package synphot in IRAF/STSDAS, although total throughput was renormalized by approximately 12% to agree with the on-orbit recalibration of the STIS CCD by Landsman (1997). This adjustment agrees well both with estimates derived by comparison of the stellar magnitudes in the WFPC2 F606W image of the GRB 970228 field with those of the STIS image and with an independent calibration of the STIS CCD performed by Sahu et al. (1997a).

The STIS CCD in clear aperture mode has a broad bandpass, with a significant response from 200 to 900 nm that peaks near 600 nm. As a result, STIS instrumental magnitudes are most accurately translated into the standard filter set by quoting the result as a V magnitude, but in any case knowledge of an object's intrinsic spectrum is required for an accurate conversion. Here we are fortunate to have an earlier image of the field in both V (F606W) and I (F814W) with the WFPC2. We therefore can use colors determined in these earlier observations to interpret the STIS data. However, to the extent that the WFPC2 colors are in error (either because of low signal-to-noise ratio or an actual change in the color of the object over time) our derived magnitudes from the STIS data will be biased by about 0.5 mag for each magnitude of error in $V - I$ (Sahu et al. 1998).

The magnitude of the optical transient (OT) was determined from the drizzled image via aperture photometry. The flux in an aperture of radius four drizzled pixels, or 0″.1, was determined, and our best estimate of the surrounding nebular background was subtracted. An aperture correc-

tion of 0.50 mag was derived for this aperture using the bright star visible in Figure 1 to the west of the nebula.

We find that the OT has a count rate of 0.206 ± 0.02 counts s^{-1} for a derived magnitude of $V = 28.0 \pm 0.25$, where the final error includes the uncertainty of the conversion to the standard photometric bandpass.

We determined the magnitude of the nebula by summing all pixels in a region of approximately 1.4 arcsec^2 surround-
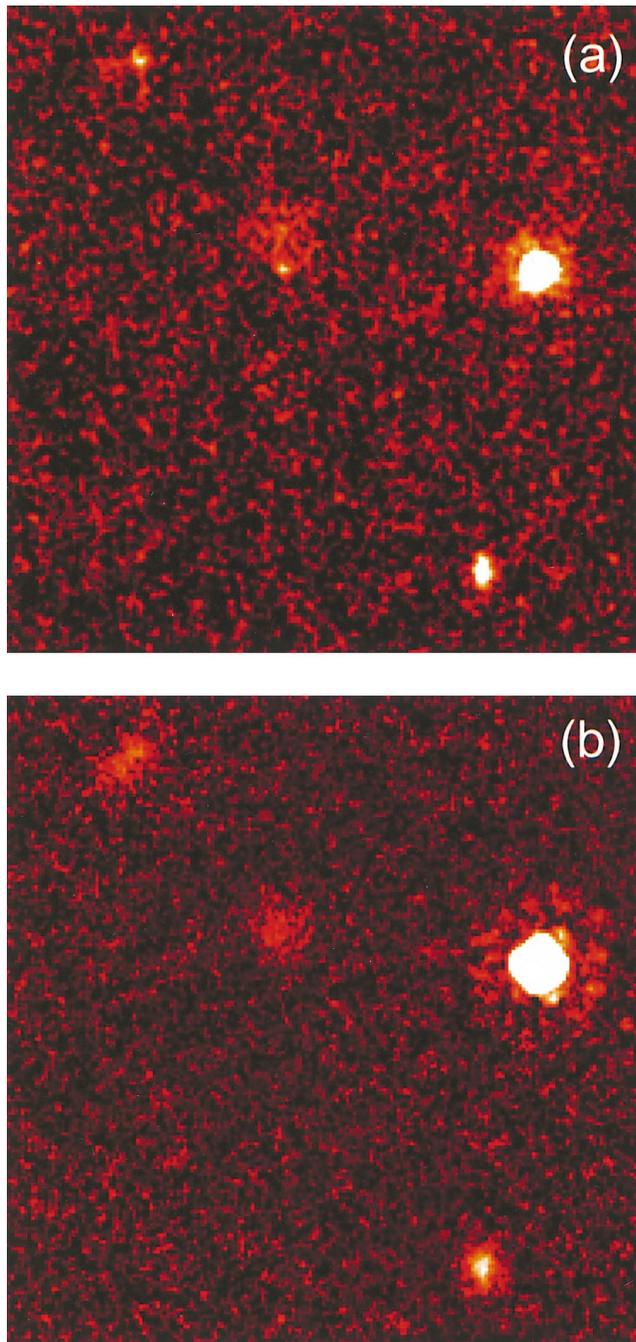
FIG. 1.—(a) STIS and (b) NICMOS drizzled images of GRB 970228. In both images, north is up and east is to the left. The images are 7″.2 on a side, and the pixel size is one-half that of the original NIC2 pixels, or about 0″.0378 pixel^{-1}. The host galaxy is the roughly circular nebulosity about 1″.5 northeast of the center of the image. The OT can be seen in the STIS image as a faint point source near the southern edge of the host galaxy. In the NICMOS image, taken approximately 6 months after the STIS image and 1 yr after outburst, the OT is no longer visible.

ing the object. The flux of the point source was then subtracted from the sum. We find a flux of 1.36 ± 0.1 counts s^{-1} and a magnitude of $V = 25.8 \pm 0.25$ for the nebula. Again, the final error is dominated by the uncertainty of the $V - I$ color of the object, for which we have only the previous, comparatively noisy, WFPC2 observations of the field (Sahu et al. 1997b).

However, the WFPC2 observations provide us with a baseline of 162 days and thus an excellent opportunity to investigate the variability and claimed proper motion of the OT, as well as to determine whether the apparent magnitude of the extended emission has remained constant.

2.2. The WFPC2 Images

In order to search for proper motion of the OT and possible changes in the apparent brightness of the extended source, we have reexamined the WFPC2 images obtained in 1997 March and April (Sahu et al. 1997b). The WFPC2 images were processed using the standard WFPC2 data pipeline, and cosmic rays were removed using the standard STSDAS task "crrej." The centroids of the four reference stars used as positional anchors by Sahu et al. (1997b) were redetermined using two-dimensional Gaussian fits to both the WFPC2 and STIS images. The positional accuracy for the reference stars is approximately 3 mas in each coordinate at each epoch, while for the relatively faint GRB it is ~ 10 mas. The measured pixel coordinates were corrected for the cameras' geometric distortion using the Roberto Gilmozzi & Kinney (1995) solutions for the WFPC2 images and a solution derived by Malamuth & Bowers (1997, STIS Calibration Report) for the STIS images. The STIS pixel coordinates were then transformed to the corresponding WFPC2 pixel coordinates, taking into account the rotation, translation, and the image scale change while assuming zero mean motion of the four reference stars. This procedure was performed on the WFPC2 V- and I-band images separately. The positions of the four stars in the WFPC2 images agree with their positions in the STIS images to within the expected uncertainties of 3 mas in both colors, which shows that the transformations between the two images have been done correctly. Averaging together all of the data we find that any motion of the GRB between the two epochs is less than 16 mas. This corresponds to a motion of less than 36 mas yr^{-1}. This is a factor of ~ 15 less than the value claimed by Caraveo et al. (1997) and improves the upper limit on the proper motion reported by Sahu et al. (1997b) by a factor of 6.

To check on the previous WFPC2 photometry of the OT and extended emission, the point-source magnitude was determined by using circular apertures of radii 1 and 3 pixels in the WFPC2 images. The values obtained were then adjusted by applying the aperture corrections and in the case of F606W, the color term for transformation to Johnson V, derived by Holtzman et al. (1995). The nebular magnitude was determined from the WFPC2 images by taking the sum of all counts above sky in a box approximately $1\rlap{.}''5 \times 1\rlap{.}''0$, and subtracting the counts (estimated as above) attributable to the point source. The position of this box was determined by the position of the nebula in the STIS image. It is, however, somewhat larger than the observed nebula in all directions. Averaging together the two WFPC2 observations, we obtain magnitudes for the extended emission of $I = 24.4 \pm 0.2$ and $V = 25.8 \pm 0.2$.

This visual magnitude is remarkably consistent with the STIS measurement.

2.3. The NICMOS Images

On 1998 February 24 we obtained a total integration time of $\sim 10,000$ s, over four orbits, on the field of GRB 970228 using the F160W (H) filter of NICMOS Camera 2. A similar set of exposures in the F110W (J) filter, scheduled for the previous day, was lost when a cosmic-ray event in the NICMOS electronics caused the camera to be reset during the first of the four orbits. However, as the F160W band on NICMOS is extremely sensitive and provides greater leverage in wavelength than the F110W filter when compared with WFPC2 and STIS imaging, the observations in hand remain immensely useful.

Each of the four orbits was subdivided into a single 512 s and two 1024 s exposures, with two dither positions performed each orbit. All exposures were taken using multiple initial and final reads, or MIF sequences. In all, eight dither positions were placed roughly along a $\sim 1''$ diagonal line. The images were processed using a variant of the standard NICMOS pipeline. "Superdark" reference files were produced for the MIF512 and MIF1024 sequences using a sigma-clipped average ($3\,\sigma$) of 20 MULTIACCUM on-orbit darks in each sequence, taken in 1997 November. First an estimate of the thermal background, the pedestal (a constant offset in each of the four chip quadrants), and shading (effectively a ramp in bias across each quadrant) were subtracted from the MULTIACCUM sequences. Then flatfielding, cosmic-ray rejection, and conversion to count rates were performed. When the final images were combined using Drizzle, noticeable streaking along the diagonal of the dither, as well as large-scale noise, remained, even after further image defects and residual cosmic rays were removed using the cosmic-ray rejection scheme described by Fruchter & Hook (1997).

We therefore created "sky" images using a technique very similar to that employed by ground-based infrared astronomers. First, the median of all MIF1024 and MIF512 images was separately obtained while masking out the astrophysical objects detected in the drizzled image previously created. These images revealed significant structure in the sky that differed substantially between the MIF512 and MIF1024 images. We therefore created an individual sky for each image by taking the median of all the other images of the same exposure time while masking regions known to include astrophysical objects in the first drizzled image. We found that four MIF512 images were insufficient to make acceptable sky images; however, the sky subtraction appeared to work well for the MIF1024 images. The final combination of the eight sky-subtracted MIF1024 images shows no evidence of correlated noise along the direction of the dither pattern, and the noise on arcsecond scales has been reduced by more than a factor of 2. Furthermore, since the individual images are read noise limited, the neglected MIF512 images represent only about one-eighth of the total signal-to-noise ratio of the data, and therefore their loss does not significantly affect the final signal-to-noise ratio that can be achieved.

The extended emission can be clearly seen in the NICMOS image displayed in Figure 1. The same $1\rlap{.}''5$ aperture as used in the WFPC2 image reveals a total count rate of 0.23 ± 0.02 counts s^{-1} in the NIC2 F160W filter, which corresponds to 470 ± 50 nJy or a magnitude of

$H = 23.21 \pm 0.1$. There is no sign of the OT in the NICMOS image; we find a 3 σ upper limit on the flux density of the OT of $H \geq 25.9$ or 40 nJy.

2.4. The Keck Images

Images of the GRB 970228 field were obtained in the K band on 1998 April 8 with the Keck I 10 m telescope and NIRC (Matthews & Soifer 1994). A 9 point pattern mosaic of individual 10 s exposures was obtained and co-added to produce an image with total exposure time of 2160 s. The resulting image point-spread function measured $0\farcs6$ FWHM. The flux of the extended source was measured inside a $1\farcs5$ diameter aperture centered on the source, and an approximate aperture correction to $4''$ was made using the curve of growth of the nearby star. Calibration was performed using the infrared standards of Persson et al. (1998), including an air-mass correction term. We obtain $K = 22.8 \pm 0.3$ or 500 ± 150 nJy. Thus, within the errors, the spectrum of the extended emission is flat in f_ν between H and K.

2.5. The New Technology Telescope Images

We have also reexamined the New Technology Telescope (NTT) observation of March 13 (Galama et al. 1997) to further test whether the nebular magnitude may have varied with time. As in the case of our analysis of the STIS image, we have again used the stellar image $\sim 2\farcs5$ to the east of the OT as a point-spread function. We find that we can subtract a point source from the position of the OT and leave behind a "nebula" as faint as, or fainter than, the extended emission in the HST/STIS image without producing any noticeable sky subtraction errors. Thus, we find no evidence that the nebula has faded with time. A complete list of photometric results can be found in Table 1.

3. DISCUSSION

3.1. The Galactic Extinction in the Direction of GRB 970228

GRB 970228 lies in the direction of $l = 188.9$ and $b = -17.9$. As a result, its apparent visual magnitude and color are significantly affected by interstellar extinction in our galaxy. Therefore, we have used several techniques to estimate the foreground Galactic extinction in its direction, so that we can obtain the true colors and unextincted magnitudes of the OT and the surrounding nebulosity. The colors and counts of background galaxies suggest $A_V \sim 0.6 \pm 0.2$ (González et al. 1998). The catalogs of Burstein & Heiles (1982) and Schlegel et al. (1997) give 0.8 and 0.75,
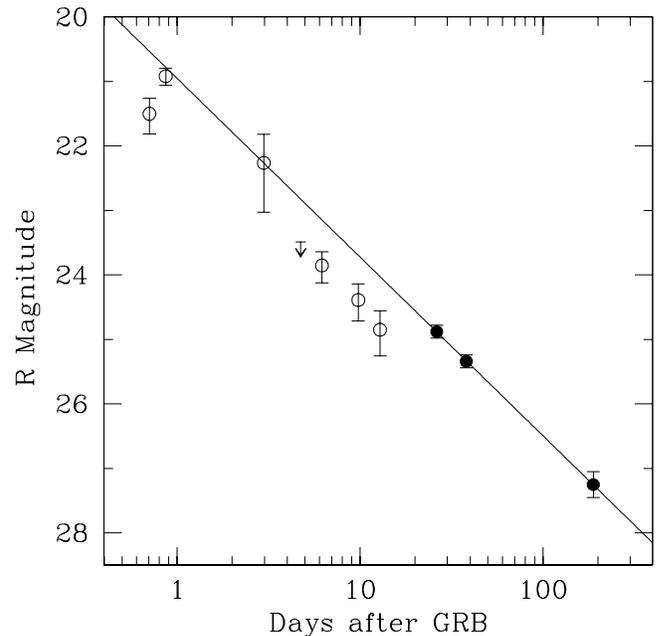

FIG. 2.—R magnitude of the OT as a function of time. Ground-based measurements are represented as open circles, and HST points as filled circles. A nebular R magnitude of 25.3 has been subtracted from all the non-HST magnitudes, which have been taken from Galama et al. (1998) and Masetti et al. (1998). An error corresponding to the uncertainty in the nebular magnitude has been added in quadrature to the ground-based errors. The line shows the best-fit power law (index 1.1 ± 0.1) through the three HST observations. Upper limits determined by ground-based telescopes have been reported only if falling below the power-law curve.

respectively, with errors of approximately 0.15 mag. The color of a background K4V star in the field suggests $A_V = 0.9 \pm 0.2$, and the Na I absorption in its spectrum implies a strong upper limit of ~ 1.0. For the remainder of this paper then, we will use the value $A_V = 0.8 \pm 0.2$, which is roughly the average of the estimates. However, because this value is noticeably less than that published by Castander & Lamb (1997), we discuss our derivation of the extinction in detail in the Appendix.

3.2. The Time History and Spectral Behavior of the Optical Transient

In Figure 2 we plot the magnitude of the OT as a function of time since the burst on 1997 February 28. The STIS magnitude has been converted to R using the color determined from the WFPC2 V and I observations. A power law

TABLE 1

OPTICAL AND NEAR-INFRARED PHOTOMETRY OF GRB 970228

| | | | JOHNSON-COUSINS MAGNITUDES | |
INSTRUMENT	BAND	DATE (UT)	Optical Transient	Nebulosity
HST/WFPC2	F606W/V	1997 Mar 26	26.05 ± 0.07[a]	25.8 ± 0.3
HST/WFPC2	F814W/I	1997 Mar 26	24.10 ± 0.07	24.6 ± 0.3
HST/WFPC2	F606W/V	1997 Apr 7	26.35 ± 0.10	25.7 ± 0.3
HST/WFPC2	F814W/I	1997 Apr 7	24.65 ± 0.10	24.3 ± 0.3
HST/STIS	50CCD/V	1997 Sep 4	28.00 ± 0.25	25.8 ± 0.25
HST/NICMOS2	F160W/H	1998 Feb 24	>25.9[b]	23.2 ± 0.1
Keck/NIRC	K	1998 Apr 8	...	22.8 ± 0.3

[a] Errors represent 1 σ uncertainties.
[b] 3 σ upper limit.

of the form $f(t) = a_0 t^\alpha$ has been fitted to the *HST* points and extrapolated back to earlier times. We find a best fit of $\alpha = -1.10 \pm 0.1$. A host *R* magnitude of 25.3 has been subtracted from all non-*HST* magnitudes. This is the *minimum* host *R* brightness consistent with an interpolation of the *V* and *I* data. If the host is in fact somewhat brighter than this, a proper subtraction would leave the first few points on the plot virtually unchanged but would somewhat *increase* the discrepancy between the power-law extrapolation and the points taken 4–11 days after outburst. The outlying points were taken at different observatories and reduced by different groups of observers. One of these points is, in fact, the NTT data that we have ourselves rereduced as described above. We do not believe that these points can be discounted.

Keck observations of GRB 970228 taken on 1997 March 30 and 31 showed total magnitudes, for the sum of OT and host, of $K = 22.0$ and $J = 23.5$ (Soifer et al. 1997). This *K*-band magnitude is about a factor of 2 greater than seen in our observations, 1 yr later. Therefore, it would appear that in late 1997 March, the optical luminosity in *K* was equally divided between OT and extended emission. Similarly, if we interpolate the *J* and *K* values to estimate an *H* magnitude in late 1997 March and compare this with the observed *HST* F160W magnitude, we again find that the power in the object is equally divided between host and OT. Furthermore, the estimated *H* and *K* flux densities for the OT on March 30 are equal within the errors with an average value of ~ 500 nJy.

Because the OT appears to have followed a power-law decline between 1997 March 26 and 1997 April 7, we can use the power law to interpolate the F814W to the 1997 March 31. Remarkably, one finds that the F814W flux density is 500 ± 50 nJy. Thus, the spectrum of the OT is flat in f_ν between 800 and 2200 nm. In contrast, even after correcting for foreground Galactic extinction, the $V - I$ color of the OT implies a spectrum $f_\nu \propto \nu^{-3}$. Unfortunately, we do not have infrared magnitudes for the OT at other times, and therefore we cannot tell whether this break in the spectrum is constant with time or whether it results from strong temporal variability of the OT in the infrared. It is certainly too abrupt, however, to be due to extinction in a host galaxy. While strong theoretical arguments exist for expecting temporal variability in the OT (Mészáros, Rees, & Wijers 1998; Rees & Mészáros 1998) it is far from clear that the variability that would be required (at least a factor of 3–6) could occur in one region of the spectrum, while another, an octave away, was unaffected. However, a break in the spectrum at 1 μm, or 3×10^{14} Hz, is also not expected at late times in the standard model (see, for example, Sari, Piran, & Narayan 1998), nor is it seen in the well-studied (and well-behaved) spectrum of GRB 970508 (Galama et al. 1998b).

Nonetheless, the fact that for over 180 days, the OT behaved roughly as the predicted power law (Wijers, Rees, & Mészáros 1997) is quite remarkable—for as the fireball of the burst expands, it sweeps up the material of the interstellar medium (ISM) surrounding it, and its power-law expansion should falter when it has absorbed an ISM rest mass comparable to the energy of the initial explosion, or when

$$t \approx 1 \text{ yr} \left(\frac{E_{52}}{n} \right)^{1/3}, \quad (1)$$

where E_{52} is the initial energy of the explosion in units of 10^{52} ergs and n is the density of the surrounding medium in protons cm^{-3}. However, were the GRB a Galactic rather than an extragalactic phenomenon, the amount of energy available would only be of order 10^{41} ergs and for any imaginable density the break would occur on a timescale of days rather than many months, although as noted by Panaitescu & Mészáros (1998), this break can be mitigated by a significantly nonspherical outflow geometry. Nonetheless, the power-law fit is in itself an argument for the extragalactic nature of the burst and thus is in agreement with all the other evidence presented in this paper.

3.3. *The Nature of the Host*

If the extended emission under the OT is truly a host galaxy, rather than, as has been proposed, a reflection nebula from an explosion in our own galaxy (Castander & Lamb 1998), then one would expect it to have a size and color that is reasonable for a galaxy of its magnitude. On the other hand, if a large fraction of the sky is covered by galaxies whose observed properties are similar to the proposed host, then even if the nebulosity is shown to be a galaxy, one would still have little evidence that it is indeed the host, rather than a chance superposition of a galaxy along the line of sight.

We have therefore compared the observed extended emission with galaxies found in the HDF. After adjusting for the differing depths and pixel sizes of the STIS and HDF images and the extinction in the direction of GRB 970228, we find that only $\sim 2\%$ of the HDF is covered by galaxies of comparable or greater surface brightness of the putative host (25.3 mag arcsec^{-2}). This result is similar to, but tighter than, that of Sahu et al. (1997b) and implies that the probability of a chance superposition is negligible. Furthermore, we find that the area on the sky of the proposed host (~ 0.5 arcsec^2) is near the median of galaxies of similar magnitude in the HDF. The most remarkable result, however, arises when we compare the color of the host with that of other galaxies in the HDF. In Figure 3 we show the spectral energy distribution of the host galaxy and compare it with the colors and magnitudes of objects in the HDF. The *H*- and *K*-band HDF magnitudes are from KPNO/IRIM observations of the HDF (M. Dickinson 1997).[14] The F606W images of the HDF have been convolved to the ground-based resolution and colors determined using isophotal magnitudes. We use AB magnitudes here rather than Vega magnitudes to conform to other work that has been done on the HDF.[15]

As can be seen in Figure 3, the host of GRB 970228 is unusually blue. Indeed, it is as blue as any galaxy in the KPNO/IRIM HDF. Although the completeness limit of this sample is slightly brighter than the magnitude of the host, *HST*/NICMOS observations recently performed on the HDF should soon allow us to test this relation on a sample that has a limiting magnitude safely below the host magnitude. Additionally, we find that the host is too blue to be fitted by shifting local galaxy templates (Coleman, Wu, &

[14] See http://www.stsci.edu/ftp/science/hdf/clearinghouse/irim/irim_hdf.html.

[15] AB magnitudes are defined by the relation mag$_{AB}$ = $-2.5 \log (f_\nu)$ + 23.9, where f_ν is given in μJy. The zero point of the AB magnitude system, unlike the Vega magnitude system, does not depend on wavelength; however, the zero point of the AB magnitude system has been set so that it agrees with the Vega magnitude system in *V*.
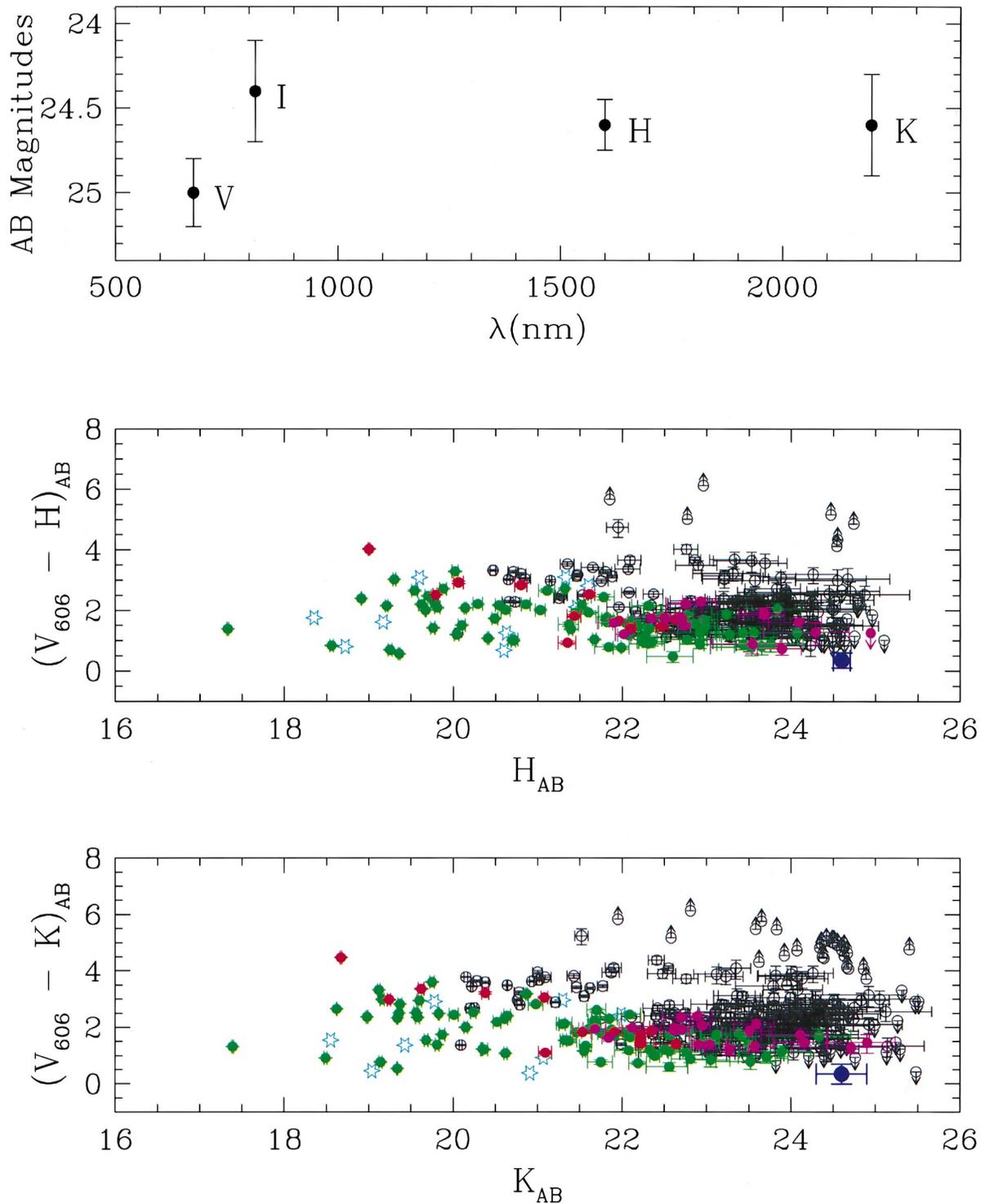
FIG. 3.—In the upper panel, the extinction-corrected spectral energy distribution of the host galaxy is shown. In the bottom two panels, we place the host galaxy on a color-magnitude diagram of objects in the HDF. Stars are shown as light blue stars. Galaxies in the HDF with spectrophotometric redshift are shown in green for $0 < z < 1$, red for $1 < z < 2$, and magenta for $z > 2$. The host galaxy is shown in dark blue. Upper and lower limits are shown with arrows.

Weedman 1980, including blue irregular dwarfs, such as the Magellanic Clouds) to higher redshift. Therefore, to attempt to fit the host's colors, we created a grid of synthetic stellar populations as described by Babul & Ferguson (1996). The models used a Salpeter IMF from 0.6 to 100 $M_\odot$. Metallicities ranged from solar to 0.05 solar. The e-folding times of the starburst were varied from 10^6 to 10^{10} yr, and the age at time of observation from 10^6 to 10^{10} yr. The stellar popu-

lations were given internal extinctions from 0 to 2 mag in A_V. If we require only that a synthetic galaxy agree with the observed colors to within the photometric errors [$\chi^2(3) < 4$], we can create galaxies of nearly any age and redshift that match. However, if we also require that the synthetic galaxy lie within the locus of observed galaxies seen in Figure 3 (because of the photometric errors, a galaxy could match the host without lying inside the locus), the set

of possible populations is dramatically reduced. All stellar populations older than 2×10^8 yr that match have essentially constant star formation rates (the time of observation is much smaller than the e-folding time of the burst); furthermore, these model galaxies cluster around two redshifts, $z \sim 0.8$ and $z \sim 4.2$. In the former case, the model is placing the 4000 Å break between F606W and F814W, and in the latter case the F606W flux is suppressed by the Lyα forest. Interestingly, at a redshift of $z \sim 0.8$ the magnitude of the host would imply an intrinsic luminosity comparable to that of the Large Magellanic Cloud and based on its photometry (and a conversion of UV luminosity to star formation rate [SFR]) (Kennicutt 1998) would have an SFR of ~ 0.5 $M_\odot$ yr^{-1}, assuming $H_0 = 65$ km s^{-1} and $\Omega = 0.3$; however, at $z \sim 4$, it would be unusually luminous—noticeably brighter than any of the photometrically identified $z \sim 4$ candidates in the HDF (Madau et al. 1996)—and have an SFR of ~ 13 $M_\odot$ yr^{-1}.

One can perhaps further limit possible host galaxies using an absence of evidence: in spite of the expenditure of many hours of spectroscopic time on Keck, this object apparently displays no emission lines. However, a young starburst—or even a continuous starburst—should show [O II] (3727 Å) emission (Kennicutt 1992) and in many cases would show Lyα (1216 Å) (Steidel et al. 1996), although this line can be suppressed by resonant scattering and absorption. For those lines to be present, yet unobserved, the redshift of the host would need to be in the range $1.3 < z < 2.5$, where O [II] has left the optical spectroscopic window in the red, yet Lyα has not yet entered in the blue. Thus, the continuous star formation models mentioned above are probably ruled out. The reason for the extraordinary blue color of the host is most likely the obvious reason—it is forming stars at an extraordinary rate for its mass. Indeed, all of the preferred stellar population models predict that the doubling time of the stellar mass is $\lesssim 2 \times 10^8$ yr, and it is this doubling time, rather than the SFR of the host, which will best indicate whether the photometry suggests that GRBs are linked with star formation. Indeed, from the slope of faint galaxy counts it can be inferred that in the range $1 \lesssim z \lesssim 3$ the luminosity function of galaxies must have been far steeper than is found locally (Hogg 1998; Hogg & Fruchter 1998). Thus, the majority of star formation at these redshifts may be found in galaxies with luminosities (and SFRs) well below L_*, the knee of the luminosity function (Schechter 1976). Therefore, if GRBs are associated with star formation, it will be the colors (and stellar lines) rather than the absolute luminosities of the hosts that will provide the proof.

Additionally, the comparison of the extinction-corrected color of the host with the HDF provides a good indication that we have not underestimated the foreground Galactic extinction. A larger A_V than the 0.75 used would have made the object bluer and caused it to lie even further outside the locus of objects seen in the HDF. Indeed, comparison with the HDF suggests that the somewhat lower extinction of

$A_V = 0.6$ implied by the comparison of the colors of background galaxies may have been closest to the correct extinction. However, even if we were to reduce the assumed extinction to match this estimate, the host would remain unusually blue.

3.4. Star Formation and GRBs

Although the host of GRB 970228 may be the first host galaxy to have sufficient published multicolor imaging to allow one to constrain the SFR, it is not the first host with strong evidence of star formation. All three GRBs with measured cosmological redshifts lie in hosts that display prominent emission from lines associated with star formation, and in all three cases the strength of those lines is high for galaxies of comparable magnitude and redshift (Djorgovski et al. 1998; Kulkarni et al. 1998a; Bloom et al. 1998a). Although other host galaxies have been observed spectroscopically (S. R. Kulkarni and R. M. Metzger 1998, private communications), the fact that no other hosts show lines is not necessarily an argument against strong star formation in these galaxies. As noted by Hogg & Fruchter (1998) reasonable models of the cosmological density of GRBs with redshift predict a substantial fraction in the range of $1.3 < z < 2.5$ where, as mentioned earlier, no strong lines are found in the optical spectroscopic window. Thus, one can argue that in all cases where the observations allow one to determine the SFR, that rate has been found to be high.

Unfortunately, our data do not allow us to distinguish between the two leading candidates for the creation of bursts, a binary neutron star (Narayan, Paczyński, & Piran 1992) and hypernovae (Paczyński 1998), as binary neutron star coalescence should occur on a timescale comparable to that of many star bursts ($\sim 10^8$ yr; Livio et al. 1998). The primary difference one expects for these two models is that because of kicks imparted to the neutron stars at birth, neutron star binaries should occasionally be well outside of a galaxy when the burst occurs (Bloom, Siggurdsson, & Pols 1998b). However, at present, we are only able to localize bursts using X-ray, radio, or optical afterglows. Yet the strength of the afterglow may depend critically on the density of the surrounding medium (Mészáros & Rees 1997). The low-density medium of intergalactic space may be too tenuous to produce detectable afterglows. In this case, deciding between binary neutron stars and hypernovae as the progenitors of GRBs may require a new generation of space observatories capable of localizing the burst on the basis of gamma rays alone.

APPENDIX A

THE FOREGROUND GALACTIC EXTINCTION TOWARD GRB 970228

In this Appendix we present several different independent methods that we have used to estimate the extinction in the direction of GRB 970228. We have consulted the extinction catalogs of Burstein & Heiles (1982) and Schlegel et al. (1997), and

we have attempted to determine directly the extinction from the counts and colors of galaxies in the WFPC field, as well as from spectroscopy and imaging of Galactic stars in the field. All these methods give consistent results.

A1. ALL-SKY EXTINCTION MAPS

Burstein & Heiles (1982) have used measured H I column densities and an empirically determined constant of conversion between H I to extinction, in combination with background galaxy counts to derive a map of Galactic extinction with a spatial resolution of about $0°.6$. Based on their work, the extinction in the direction of GRB 970228 is $A_V = 0.8 \pm 0.1$. Similarly, Schlegel et al. (1997) have used the *IRAS* 100 μm maps to estimate foreground Galactic extinction, with an angular resolution of $\sim 6'$. Their work implies an extinction of $A_V = 0.75 \pm 0.15$. The consistency of these numbers is encouraging and, as will be seen, agrees well with our other estimates.

A2. GALAXY COUNTS AND COLORS

Foreground extinction should be visible as a diminution in the number counts of galaxies in the field to a given limiting magnitude and a reddening of those that are detected. We therefore have compared the WFPC2 images of the GRB 970228 field with those of four high latitude fields taken from the *HST* archive, the HDF (Williams et al. 1996), the field around the weak radio galaxy 53W002 (Pascarelle et al. 1996), and the fields at $\alpha_{2000} = 15^{\rm h}58^{\rm m}49^{\rm s}.8$, $\delta_{2000} = 42°05'23''$ and at $\alpha_{2000} = 14^{\rm h}17^{\rm m}43^{\rm s}.63$, $\delta_{2000} = 52°28'41''.2$ imaged by Westphal and collaborators as part of *HST* proposal 5109. In the case of the HDF, the distributed drizzled images were used. In all other cases we reduced the data ourselves, again producing a drizzled output. Further details of the data reduction technique can be found in González, Fruchter, & Dirsch (1998).

The SExtractor object extraction software (Bertin & Arnouts 1996) was used to locate objects, perform star-galaxy separation, and obtain photometry on galaxies. Objects were extracted down to a limiting surface brightness in the F606W images of 25 mag arcsec^{-2}, which was determined by the shallowest image (that of the GRB field). Colors were obtained by placing matching fixed size apertures of diameter $0''.4$ on the F814W fields. To simulate extinction the limiting magnitude was progressively raised in the reference fields until the number counts and colors matched those of the GRB field. A more detailed account of the actual fitting procedure can be found in González et al. (1998).

Comparison of the counts in the GRB field with those of the HDF and 53W002 field gives a best estimate of extinction of $A_V \sim 0.7 \pm 0.2$; however, the two Westphal fields have significantly fewer galaxies, by an amount that is large compared with the expected clustering error (although, as discussed by González et al. 1998, this error may be generally underestimated). If these two fields are averaged in with the HDF and 53W002 fields, the best value of extinction is $A_V = 0.5 \pm 0.2$. Although the counts differ, the colors of background galaxies in these four fields agree well. The extinction implied by the average color difference between the GRB field and the four background fields is $A_V = 0.6 \pm 0.1$, where the error is the measured dispersion in estimated extinction between the four reference fields using the color index. However, there may be a slight bias in the color estimation—if the reddening is clumpy, the most reddened background galaxies may fall out of the sample and not affect the average color. Thus, the estimate of $A_V = 0.6$ should probably be viewed as a lower limit. In any case, this estimate is in good agreement with the Burstein & Heiles (1982) and Schlegel et al. (1997) extinctions.

A3. STELLAR SPECTROSCOPY

We have also examined the long-slit spectra of the GRB 970228 field obtained by Tonry et al. (1997), and generously made available on the World Wide Web, to estimate the extinction to GRB 970228. The observations were done using the LRIS spectrograph mounted on the Keck II telescope. The final combined spectrum covers the wavelength range 4320–9300 Å at a spectral resolution of 11 Å (FWHM). The total exposure time was 5000 s, and the weighted mean air mass was 1.52. The slit was $1''$ wide. We performed flux calibration using a spectrum of spectrophotometric standard star Hiltner 600 (Hamuy et al. 1994) with the same slit width. Three stars are present in the slit of the Tonry et al. spectrum, denoted S1, S2, and S3 (see Tonry et al. 1997). Before extracting the spectra of these stars, we corrected the summed long-slit spectrum for tilt and geometric distortion by measuring the centroids of the stars along the slit as a function of wavelength. The table of centroid positions was then used to rectify the long-slit spectra, using IRAF tasks geomap and geotran. The star spectra were subsequently extracted using an "optimal extraction" algorithm, described by Horne (1986).

The slit in these observations falls along two K stars in the PC field of the WFPC2 images (denoted as S1 and S2 as in Tonry et al. 1997), as well as on the GRB itself. The brightest of these two stars can be clearly identified as a K4V, and it is likely that the other is also a K4V. Like Castander & Lamb (1998), we have attempted to fit the observed Keck continuum by applying varying extinctions to library K4V spectra (Jacoby, Hunter, & Christian 1984; Silva & Cornell 1992). *We find no satisfactory solution.* We cannot match the slope across the entire continuum no matter what extinction we use (examples of poor fits can be seen in Fig. 3 of Castander & Lamb 1998). This may be due partially to the fact that the position angle of the slit was approximately $45°$ from the parallactic angle. However, this cannot entirely account for the effect. It appears possible that the stars were partially off the slit and/or that the publicly available flat field does not provide a true spectrophotometric correction.

While we may not be able to properly flatten the Tonry et al. (1997) spectra on large scales, this should not significantly affect our ability to examine the equivalent widths of lines in the spectrum. In particular, we can use the equivalent width of the interstellar Na I D doublet ($\lambda\lambda 5890, 5896$) to place a limit on the reddening in the field.

In the ISM gas and dust grains are generally associated with one another. This was recognized in the 1940s from the correlations between the intensity of the interstellar Na I D doublet and the reddening of starlight (e.g., Spitzer 1948). Indeed, observations of stars at intermediate and high Galactic latitudes indicate that the column density of interstellar Na I is correlated with $E(B-V)$ (Cohen 1974; Hobbs 1974b; Ferlet, Vidal-Majar, & Gry 1985).

This relationship shows, however, a rather significant scatter, which can be understood as being due to *spatial* variations: for disk stars behind or within dense dark clouds in the solar neighborhood, the equivalent width (EW) of interstellar Na I in spectra of stars is smaller (for a given amount of reddening) than those of more distant stars at high Galactic latitude. This is due to Na I depletion in dense clouds, where many heavy elements must be locked onto dust grains (e.g., Cohen 1973). Another contributor to the scatter in the EW(Na I) versus $E(B-V)$ relationship (at high column densities) is the effect of ionization: as the cloud density increases the ratio of neutral to ionized gas increases proportionally, causing *enhanced* Na I absorption for a given $E(B-V)$ (Hobbs 1974b).

In order to quantify the interstellar Na I absorption versus reddening relationship, we show in Figure 4 EW(Na I) against $E(B-V)$ for a large number of early-type (O and early B) stars taken from the literature (Cohen 1973, 1974, 1975; Hobbs 1974a, 1978; Ferlet et al. 1985). So that we could compare these data with the Tonry et al. spectra, which were obtained with a lower dispersion, we selected stars for which both components of the Na I doublet were measured. Figure 4 depicts these data for different lines of sight: (1) nearby stars within or behind dense clouds, (2) distant supergiant stars for which the line of sight goes through the low-density intercloud medium, and (3) stars at high Galactic latitude, for which the reddening arises most probably from the disk layer with a half-thickness of 100 pc (Cohen 1974). Case 2 is arguably the most appropriate for the line of sight to GRB 970228, since Galactic globular clusters at low latitude show a similar relation between EW(Na I) and $E(B-V)$ (Bica & Alloin 1986).

In K main-sequence stars such as S1 and S2, the Na I D absorption line strength is partly due to the stellar photosphere. Furthermore, the contribution of the stellar photosphere to the total line strength is a function of stellar metallicity. To quantify the stellar contribution, we have measured the EWs of the Na I D doublet as well as the Mg I b triplet (which is a measure of stellar metallicity and unaffected by the ISM) for stars S1 and S2 and compared them with those of the library K4V star from Silva & Cornell (1992). The wavelength intervals for the line indices were taken from Burstein et al. (1984). The results are listed in Table 2.

It is evident from Table 2 that stars S1 and S2 are more metal rich than the library K4V star and yet have Na I D EWs that are at most marginally larger. The straightforward interpretation of this result is therefore that the interstellar contribution to EW(Na I D) [hereafter EW(Na I D)$_{ISM}$] for stars S1 and S2 is consistent with zero.
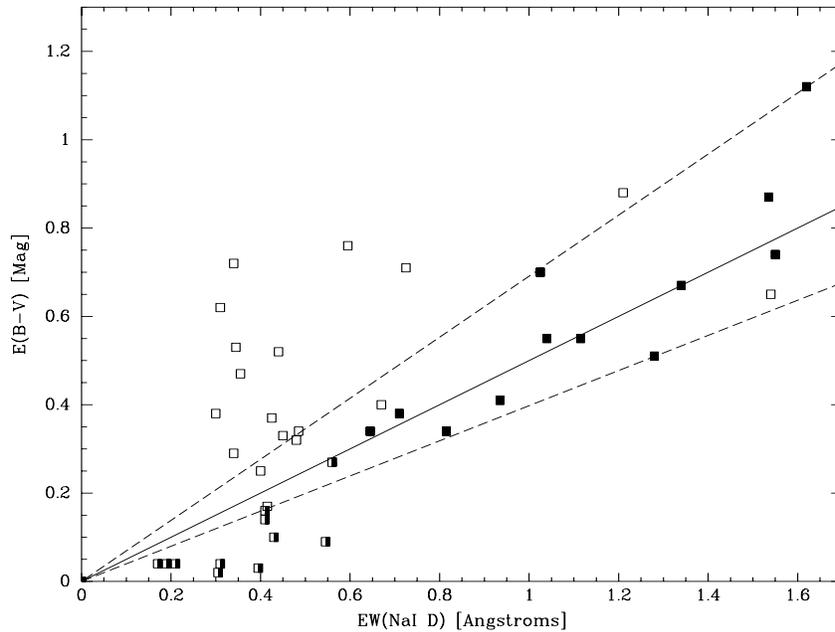

FIG. 4.—Equivalent width of Na I D absorption line against $E(B-V)$ for stars along different lines of sight. Open symbols are for nearby stars within or behind dense clouds in the solar neighborhood, half-open symbols are for stars at medium to high Galactic latitude, and solid symbols are for distant supergiant stars for which the line of sight goes through the low-density intercloud medium. The solid line is a linear least-squares fit to the data on the latter category of stars, and the dashed lines delineate the extreme possible slopes of that relation. See text for discussion.

TABLE 2

Na I AND Mg I EQUIVALENT WIDTHS
(IN ANGSTROMS)

Star	EW(Na I D)	EW(Mg I b)
S1	6.1 ± 1.0	9.0 ± 1.0
S2	6.2 ± 0.2	8.4 ± 0.2
K4V[a]	6.0 ± 0.1	7.1 ± 0.1

[a] Library star from Silva & Cornell 1992.

To derive a stringent upper limit to EW(Na I D)$_{\rm ISM}$, we used the Na I D profile of the K4V library star as a template (i.e., purely stellar) spectrum and evaluated the maximum "extra" EW that can be accommodated in the spectrum of star S2 within the errors (the spectrum of star S1 is too noisy for us to use for this purpose). The resulting upper limit is EW(Na I D)$_{\rm ISM}$ $\lesssim 0.5$ Å.

Using the relation of $E(B-V)$ versus EW(Na I D)$_{\rm ISM}$ for distant stars in the Galactic disk (depicted in Fig. 4 as a solid line, along with two dashed lines that depict the minimum and maximum possible slopes), we find that this upper limit to EW(Na I D)$_{\rm ISM}$ translates into $E(B-V) \lesssim 0.25^{+0.09}_{-0.05}$ Å, equivalent to $A_V \lesssim 0.75^{+0.27}_{-0.15}$ assuming the Galactic extinction law of Rieke & Lebofsky (1985).

A4. STELLAR COLORS

There is one further means of measuring the extinction available to us. Given that we believe star that S2 of Tonry et al. (1997) can be accurately classified as a K4V, we can examine the F606W and F814W images and compare the observed colors with those of library stars. We have done this using the IRAF/STSDAS (Tody 1993) program synphot to multiply a standard library spectrum (chosen from the libraries mentioned above) with an extinction curve and the response of the WFPC2 instrument. We find that the ratio of counts s^{-1} between the F606W and F814W images of 1.12 is fitted with an $A_V = 0.9$ $\pm$ 0.2, where the error is dominated by the choice of library spectrum and form of the Galactic extinction curve. Using a reddened library spectrum in synphot we find that S2 has an R-band magnitude of 22.85. After dereddening this would correspond, for a K4V star, to a distance of ~ 6.8 kpc. Given that this star is in the Galactic anticenter, and at a Galactic latitude of $\sim 18°$, all of the dust along this line of sight is almost certainly between us and the star. Therefore, the reddening of the star is a valid measure of the total extinction in this direction of the sky.

REFERENCES

Babul, A., & Ferguson, H. 1996, ApJ, 458, 100
Bertin, E., & Arnouts, S. 1996, A&AS, 117, 393
Bica, E., & Alloin, D. 1986, A&A, 166, 83
Bloom, J. S., Djorgovski, S. G., Kulkarni, S. R., & Frail, D. A. 1998a, Late-Time Optical Observations of Gamma-Ray Burst 970508, preprint
Bloom, J. S., Sigurdsson, S., & Pols, O. R. 1999, MNRAS, in press
Bond, H. E. 1997, IAU Circ. 6654
Burstein, D., Faber, S. M., Gaskell, C. M., & Krumm, N. 1984, ApJ, 287, 586
Burstein, D., & Heiles, C. 1982, AJ, 87, 1165
Caraveo, P. A., Mignani, R. P., Tavani, M., & Bignami, G. F. 1997, A&A, 326, L13
Castander, F. J., & Lamb, D. Q. 1998, in AIP Conf. Proc. 428, Gamma-Ray Bursts: 4th Huntsville Symposium, ed. C. A. Meegan, R. D. Preece, & T. M. Koshut (New York: AIP), 520
Cohen, J. G. 1973, ApJ, 186, 149
———. 1974, ApJ, 194, 37
———. 1975, ApJ, 197, 117
Coleman, G. D., Wu, C. C., & Weedman, D. W. 1980, ApJS, 43, 393
Djorgovski, S. G., Kulkarni, S. R., Goodrich, R., Frail, D. A., & Bloom, J. S. 1998, GCN, 139
Djorgovski, S. G., et al. 1997, Nature, 387, 876
Ferlet, R., Vidal-Majar, A., & Gry, C. 1985, ApJ, 298, 838
Fruchter, A. S., & Hook, R. N. 1997, in Proc. SPIE 3164, Applications of Digital Image Processing XX, ed. A. Tescher (Bellingham: SPIE), 120
Galama, T. J., et al. 1997, Nature, 387, 479
———. 1998a, GCN, 60
Galama, T. J., Wijers, R. A. M. J., Bremer, M., Groot, P. J., Strom, R. G., Kouveliotou, C., & Van Paradijs, J. 1998b, ApJ, 500, L97
González, R. A., Fruchter, A. S., & Dirsch, B. 1998, ApJ, 515, 000
Hamuy, M., Suntzeff, N. B., Heathcote, S. R., Walker, A. R., Gigoux, P., & Phillips, M. M. 1994, PASP, 106, 566
Hobbs, L. M. 1974a, ApJ, 191, 381
———. 1974b, ApJ, 188, L67
———. 1978, ApJS, 38, 129
Hogg, D. W. 1998, Ph.D. thesis, Caltech
Hogg, D. W., & Fruchter, A. S. 1998, ApJ, in press
Holtzman, J. A., Burrows, C. J., Casertano, S., Hester, J. J., Trauger, J. T., Watson, A. M., & Worthey, G. 1995, PASP, 107, 1065
Horne, K. 1986, PASP, 98, 609
Jacoby, G. H., Hunter, D. A., & Christian, C. A. 1984, ApJS, 56, 257
Kennicutt, R. C., Jr. 1992, ApJ, 388, 310
———. 1998, ARA&A, 36, 131
Kulkarni, S. R., et al. 1998a, Nature, 393, 35
———. 1998b, Nature, 395, 663
Landsman, W. 1997, STIS CCD Image Mode Sensitivity, Internal STIS Calibration Document
Livio, M., et al. 1998, in AIP Conf. Proc. 428, Gamma-Ray Bursts: 4th Huntsville Symposium, ed. C. A. Meegan, R. D. Preece, & T. M. Koshut (New York: AIP), 483

Madau, P., Ferguson, H., Dickinson, M., Giavalisco, M., Steidel, C., & Fruchter, A. S. 1996, MNRAS, 283, 1388
Malamuth, E., & Bowers, C. W. 1997, in HST Calibration Workshop, ed. S. Casertano, R. Jedrzejewski, T. Keyes, & M. Stevens (Baltimore: STScI), 144
Masetti, N., Bartolini, C., Guarnieri, A., & Piccioni, A. 1998, Nucl. Phys. B Proc. Suppl., 69 (1–3), 674
Matthews, K., & Soifer, B. T. 1994, in Infrared Astronomy with Arrays: The Next Generation, ed. I. McLean (Dordrecht: Kluwer), 239
Mészáros, P., & Rees, M. J. 1997, ApJ, 476, 232
Mészáros, P., Rees, M. J., & Wijers, R. A. M. J. 1998, ApJ, 499, 301
Metzger, R. M., Cohen, J. G., Chaffee, F. H., & Blandford, R. D. 1997a, IAU Circ. 6676, 3
Metzger, R. M., Djorgovski, S. G., Kulkarni, S. R., Steidel, C. C., Adelberger, K. L., Frail, D. A., Costa, E., & Frontera, F. 1997b, Nature, 387, 878
Narayan, R., Paczyński, B., & Piran, T. 1992, ApJ, 395, L83
Paczyński, B. 1998, ApJ, 494, L45
Panaitescu, A., & Mészáros, P. 1998, ApJ, submitted (astro-ph/9806016)
Pascarelle, S. M., Windhorst, R. A., Keel, W. C., & Odewahn, S. C. 1996, Nature, 383, 45
Persson, S. E., Murphy, D. C., Krzeminski, W. M. R., & Rieke, M. 1998, AJ, 116, 2475
Rees, M. J., & Mészáros, P. 1998, ApJ, 496, L1
Rieke, G. H., & Lebofsky, M. J. 1985, ApJ, 288, 618
Roberto Gilmozzi, S. E., & Kinney, E. 1995, WFPC2 Instrument Science Report 95-02
Sahu, K. C., et al. 1997a, ApJ, 489, L127
———. 1997b, Nature, 387, 476
———. 1998, ApJ, 492, L125
Sari, R., Piran, T., & Narayan, R. 1998, ApJ, 497, L17
Schechter, P. 1976, ApJ, 203, 297
Schlegel, D. J., Finkbeiner, D. P., & Davis, M. 1997, ApJ, 500, 525
Silva, D. R., & Cornell, M. E. 1992, ApJS, 81, 865
Soifer, B., et al. 1997, IAU Circ., 6619, 1
Spitzer, L. 1948, ApJ, 108, 276
Steidel, C. C., Giavalisco, M., Pettini, M., Dickinson, M., & Adelberger, K. L. 1996, ApJ, 462, L17
Tody, D. 1993, in ASP Conf. Ser. 52, Astronomical Data Analysis Software and Systems II, ed. R. J. Hanisch, R. J. V. Brissenden, & J. Barnes (San Francisco: ASP), 173
Tonry, J. L., Hu, E. M., Cowie, L. L., & McMahon, R. G. 1997, IAU Circ. 6620
van Paradijs, J., et al. 1997, Nature, 386, 686
Wijers, R. A. M. J., Rees, M. J., & Mészáros, P. 1997, MNRAS, 288, L51
Williams, R. E., et al. 1996, AJ, 112, 1335